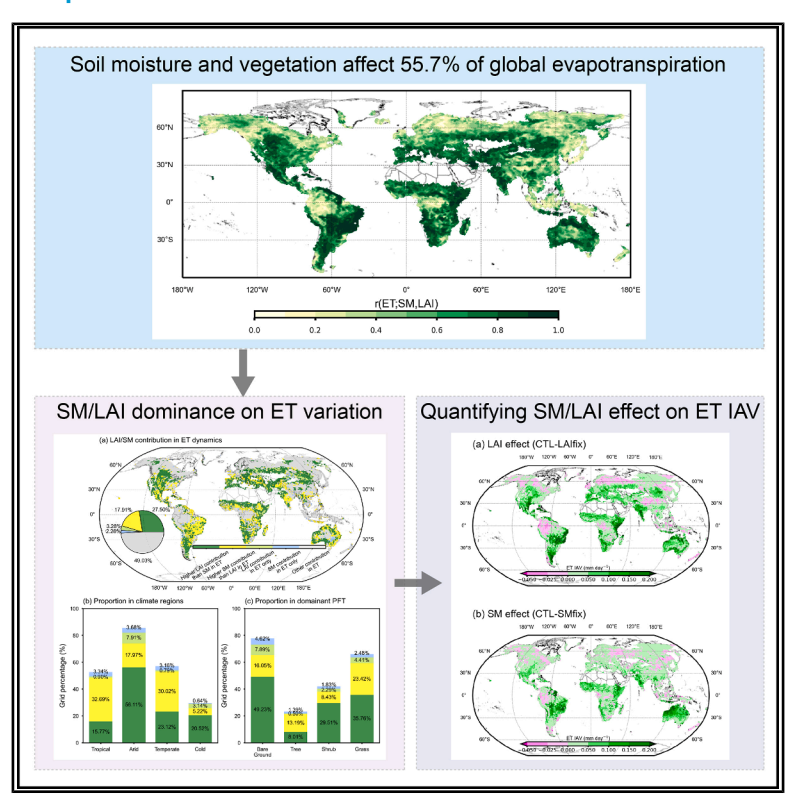
iScience

Decoupling vegetation and soil-moisture interaction in evapotranspiration interannual variability

Graphical abstract



Authors

Xiaowen Huang, Shijing Liang, Alan D. Ziegler, Zhenzhong Zeng

Correspondence

zengzz@sustech.edu.cn

In brief

Atmospheric science; Earth sciences; Environmental analysis; Environmental science; Global change

Highlights

- Soil moisture and vegetation affect 55.7% of global evapotranspiration variation
- Soil moisture controls evapotranspiration variability in lowlatitude area
- Vegetation dominates high-latitude and arid area evapotranspiration change
- Vegetation impact on evapotranspiration variability can surpass soil moisture





iScience



Article

Decoupling vegetation and soil-moisture interaction in evapotranspiration interannual variability

Xiaowen Huang, 1,2 Shijing Liang, 2,3,4 Alan D. Ziegler, 5 and Zhenzhong Zeng 1,2,6,*

*Correspondence: zengzz@sustech.edu.cn https://doi.org/10.1016/j.isci.2025.113008

SUMMARY

Evapotranspiration (ET) shapes climatic variability through the land-atmosphere coupling (LAC). While the relationship between soil moisture and ET is intuitive, the dynamical interaction among vegetation, soil moisture, and ET in LAC is understudied. Here we disentangle soil moisture and the vegetation influence on ET interannual variability using the Community Earth System Model. Globally, 55.7% of the land shows high soil moisture and vegetation coupling with ET. Soil moisture-ET coupling predominates in low-latitude LAC hotspots, while vegetation-ET coupling dominates in arid areas and high latitudes where shrubs and grasses prevail. In high-temperature and low-precipitation areas, soil evaporation induces an ET variability of 0.072 mm day⁻¹, whereas transpiration exerts stronger variability of 0.092 mm day⁻¹. The findings underscore the essentiality of vegetation in ET dynamics, suggesting that its influence may be underestimated in current LAC assessments—and that such underestimation could heighten the risk of extreme events in a warming climate.

INTRODUCTION

Evapotranspiration (ET) is a key terrestrial hydrological process that contributes to energy exchange and the carbon cycle through the transition of liquid water to the vapor phase at the surface and transfer into the atmosphere. 1-4 It is also an important linkage between the atmosphere and the terrestrial ecosystems, manifesting its role in the land-atmosphere coupling (LAC).1,5 Here the term "coupling" represents the extent to which one variable affects the other, describing a one-way control, whereas the two-way coupling is described as "feedback".1 LAC has been demonstrated to significantly amplify global warming, influence regional climate interannual variability (IAV), and directly contribute to extreme droughts and heatwave events, 2,7-9 as exemplified by the 2022 persistent compound drought and heatwaves in eastern China. 10 ET-involved LAC is 2-fold: it can couple with land components (e.g., soil moisture (SM) and vegetation) and the atmospheric variables (e.g., precipitation and air temperature). 11 As ET is composed of soil evaporation, interception, and transpiration by definition, ET can be mainly regulated by SM and vegetation dynamics, and other atmospheric contributors.3 Understanding the control of these variables in ET constitute a vital part of the ET-involved LAC and sheds light on the coupled land-climate effects. 12

Previous studies^{1,2,13,14} mainly explore the role of SM in LAC, quantifying coupling strength and uncovering the mechanisms through different measurements, such as the GLACEtype coupling strength parameter, variance analysis, and correlation analysis. By applying these measurements, the influences of LAC on temperature and precipitation are found to be mostly regulated through SM-ET coupling. 1 Strong SMclimate coupling exists in global transition zones where ET is sensitive to SM. 1,13,14 Meanwhile, the vegetation influence on regional climate is not negligible. 15,16 As vegetation increasingly governs surface energy fluxes and climate dynamics, it becomes essential to account for vegetation impacts in LAC assessments—rather than relying solely on traditional SM-based metrics. 17-19 When taking vegetation metrics into account, current estimates of LAC could be underestimated, and the area affected by LAC may extend beyond SM coupling "hotspots".

Moreover, the regulation of climate by SM and vegetation is often studied in isolation, overlooking their tight coupling and interactive feedbacks. ^{20–22} Currently needed is a better understanding of global land-ET coupling that includes the synergistic effects of both SM and vegetation (SM-vegetation-ET coupling). The complex, spatiotemporal interactions between SM and vegetation introduce additional uncertainty in diagnosing and



¹State Key Laboratory of Soil Pollution Control and Safety, Southern University of Science and Technology, Shenzhen, China

²School of Environmental Science and Engineering, Southern University of Science and Technology, Shenzhen, China

³Ningbo Institute of Digital Twin, Eastern Institute of Technology, Ningbo 315200, China

⁴Department of Building Environment and Energy Engineering, The Hong Kong Polytechnic University, Hong Kong, China

⁵Andaman Coastal Station for Research and Development, Kasetart University, Ranong, Thailand

⁶Lead contact





quantifying the relative contributions of SM-ET and vegetation-ET coupling across the global land surface.

To address these issues, we use the fully coupled Community Earth System Model 2 (CESM2)²³ to conduct a series of simulations to provide global estimations of the land-ET coupling (Figure S1). Three simulations are applied to investigate the role of SM and leaf area index (LAI) dynamics in regulating the ET variability over the historical period from 1985 to 2014. The simulations share the same configurations, with the only differences in the prescribed monthly LAI and SM time series. The control simulation (CTL) includes prescribed monthly dynamics of both SM and LAI. In comparison, the SMfix simulation uses prescribed SM climatology while allowing dynamically calculated LAI (same as the prescribed LAI dynamics in CTL), whereas the LAIfix experiment applies prescribed LAI climatology with dynamically calculated SM (same as the prescribed SM dynamics in CTL). All simulations are run from 1980 to 2014. We discard the first 5 years and restrict the analysis to 1985–2014 to ensure the simulated fields are balanced.

We adopt the multiple correlation coefficient as an indirect indicator to measure the global SM-vegetation-ET coupling strength on the inter-annual scale using annual SM, LAI, and ET data derived from CTL monthly output. The annual time series from the CTL are then used to determine the dominant contributors (SM-dominated or LAI-dominated) on ET variability with multiple linear regressions. In specific, we isolate the magnitude of the SM-dominated (LAI-dominated) effects by the ET IAV difference between CTL and SMfix (LAIfix) simulations. The magnitudes of ET IAV are measured as the value of the standard variations of the de-trended ET annual time series.

RESULTS

Overall effects of soil moisture and vegetation on ET variation

Using annual time series of SM, LAI, and ET data from the CTL output, we find that the coupling strength of SM and vegetation on ET, quantified by the multiple correlation coefficient, has great spatial variability globally (Figure 1). More than half (55.7%) of the analyzed areas with annual mean LAI >0.1 have high correlation (>0.6) between ET and both SM and LAI. Prominent areas include central South America, western North America, eastern Africa, and the zone stretching from Eastern Europe to central Asia (Figure 1A). Spatially, the ET time series has a high correlation with SM and LAI mainly in low-to-mid latitude regions, ranging from 10° to 50° in both the northern and the southern hemispheres, except for tropical rainforests, East Asia, and eastern North America (Figure 1B). The correlations between SM, vegetation, and ET in the highlatitude region (>50°N) are generally weak (<0.6). As shown in Figure 1C, on the inter-annual scale, ET is the most sensitive to SM and LAI variation in arid regions, having a mean correlation coefficient of 0.76 \pm 0.15, followed by temperate regions (0.61 \pm 0.24) and tropical regions (0.59 \pm 0.27). In addition, ET in cold areas has the lowest sensitivity to SM and LAI variabilities (0.48 ± 0.23) .

The strong coupling across different climate regions suggests widespread control of the land components on ET when accounting for both SM and vegetation (Figure 1C; also see

Figure S2). The highest coupling strength occurs in areas dominated by bare soil (0.72 \pm 0.18; Figure 1D). In climate zones that support sparse vegetation, the coupling with ET is also relatively high. For example, grasslands have the highest coupling strength (0.68 \pm 0.21), compared with shrublands (0.61 \pm 0.24). ET change in forests is generally less sensitive to SM and LAI dynamics compared with bare soil, grasslands, and shrublands, corresponding with the weak coupling strength (0.44 \pm 0.24) mainly in tropical rainforests and boreal forests (Figure 1A). Overall, ET coupling strength is influenced not only by climate regime but also by vegetation type, highlighting the varying contributions of both vegetation-ET and SM-ET coupling.

Separating SM-coupling and LAI-coupling using linear regression

We extend our analysis from SM-LAI-ET coupling in CTL simulations to separately considering vegetation-ET and SM-ET coupling effects quantified with multiple linear regressions to the annual SM, LAI, and ET time series. To exclude autocorrelation and multicollinearity between SM and LAI, we applied the variance inflation factor (VIF)²⁴ analysis and found that all VIF values between SM and LAI are nearly all below five, suggesting that our multiple linear regression method is valid (Figure S3). In general, ET dynamic in most regions is regulated by both LAI and SM, as indicated by the positive SM-ET and LAI-ET correlations. respectively. Higher SM (LAI) facilitates ET and smaller SM (LAI) reduces ET. Nevertheless, the contributions of SM and LAI display distinct latitudinal patterns (Figure S4). LAI has larger influence on ET dynamic mainly in mid-to-high latitude regions (30°N-60°N and 30°S-60°S) and in arid areas such as Africa (Figure S4A). In comparison, SM largely controls ET dynamic in low latitude regions (30°S-30°N) and eastern United States (Figure S4B).

Regions with a multiple correlation coefficient $r(ET; SM, LAI) \ge 0.6$ were retained, such that the joint effects of SM and LAI are regarded as the major contributors to the ET variations. Within these grids, we further analyzed whether SM or LAI is more dominant in the variations of ET and categorized them into four types based on the signs of the regression coefficients for LAI/SM (Figure 2). Globally, ET dynamics in 45.41% of the analyzed grids are dominated by the jointly contributions of SM and LAI. There are also areas where ET variation is dominated by SM or LAI only. In the mid-to-high latitude region of the northern hemisphere, the LAI-only type (3.28%) accounts for a larger proportion compared to the SM-only type (2.28%). The LAI-only type is identified in areas with high multiple correlation coefficients, implying strong vegetation-ET coupling (Figures 1A and 2A).

SM and LAI exert varying degrees of control on ET variation across different climatic regions (Figure 2B). In tropical areas, 52.70% of the grids are impacted by SM-ET/LAI-ET coupling. 36.03% of the grids are dominated by SM-ET coupling (32.69% for SM-dominated and 3.34% for SM-only). Meanwhile, vegetation-ET coupling is weak: LAI-dominated and LAI-only account for only 15.77% and 0.90% of the areas, respectively. The predominance of SM-ET coupling is also observed in temperate regions, accounting for 33.18% of the temperate grid cells (30.02% for SM-dominated and 3.16% for SM-only).



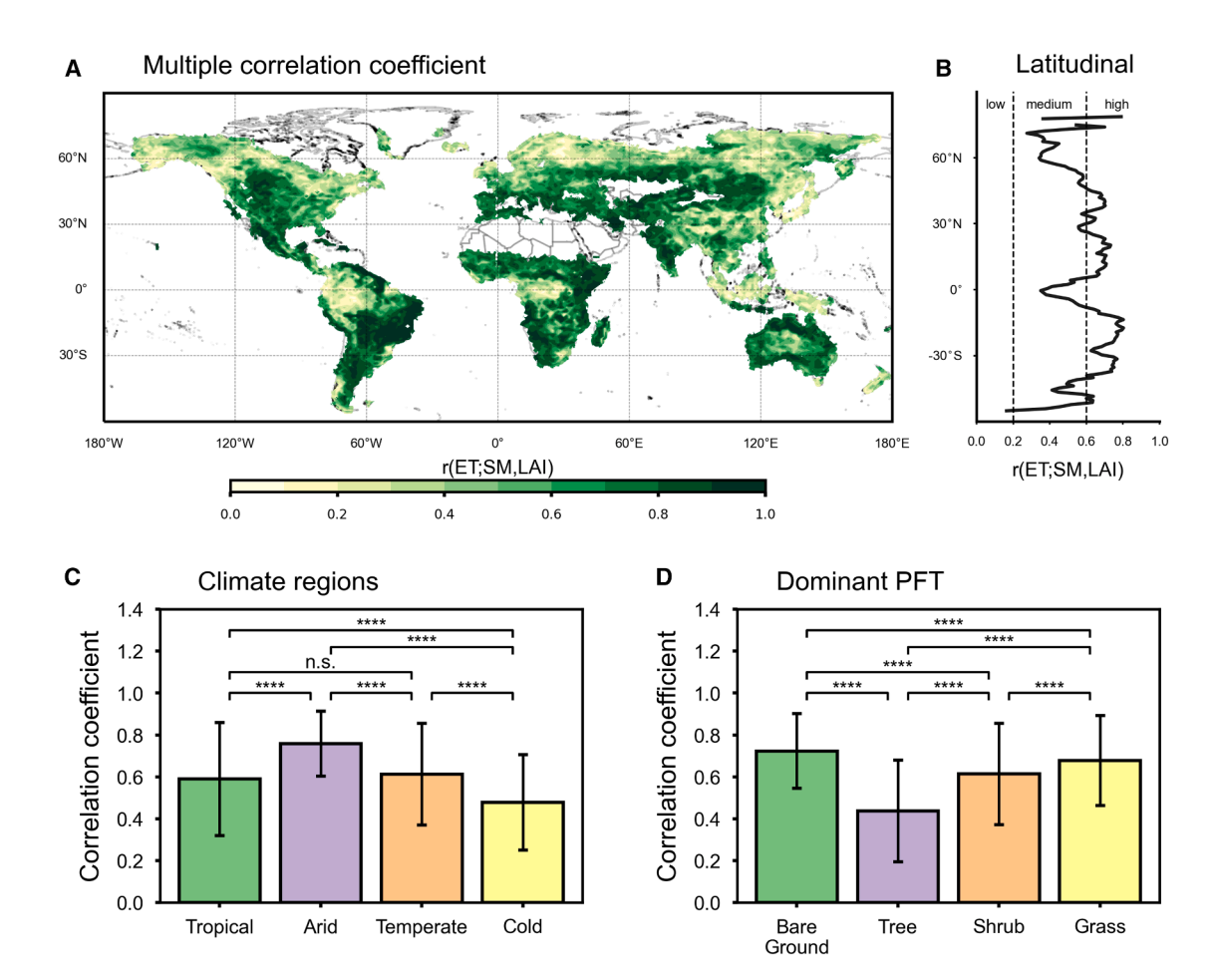


Figure 1. SM-vegetation-ET coupling strength

(A) Global spatial distribution of the multiple correlation coefficient between ET, SM, and LAI, denoted as r(ET; SM, LAI). Areas where annual LAI <0.1 are excluded.

- (B) The latitudinal distribution of r(ET; SM, LAI).
- (C) Mean r(ET; SM, LAI) for different climate regions.
- (D) Mean r(ET; SM, LAI) for different dominant plant functional types (PFT).

Error bars indicate the standard error of the mean values. The asterisks denote statistical differences in mean values (Student's t test). ****p < 0.0001; n.s. p > 0.05.

The situation changes in arid regions where 64.02% of the grids are LAI-dominated (56.11%) or solely contributed (7.91%) by vegetation-ET coupling. The prevalence of vegetation-ET coupling still exists in cold regions where 23.66% of the grids are LAI-dominated and LAI-only grids, confirming the leading role of vegetation-ET coupling in high-latitude areas compared with the small proportion of SM-ET coupling (5.86%).

Spatial differences between SM-ET coupling and vegetation-ET coupling are evident across different plant functional types (PFTs; Figure 2C). ET is more sensitive to variations in LAI and SM over bare ground and grasslands, where 77.79% and 66.07% of grid cells, respectively, are dominated by either LAI or SM effects. Specifically, LAI is more prevalent in inducing ET variation in bare ground, shrublands, and grasslands where LAI values are small. As for the forests, SM variability is more responsible for ET change, but the overall coupling is weak as only 23.09% of the grids are regulated by SM (14.58%) or LAI (8.51%). The LAI dominance on grassland is further supported

within each climate region: a higher proportion of grassland is involved in strong LAI-ET coupling than in SM-ET coupling across tropical, arid, and cold regions, whereas higher proportion of tree is more frequently associated with strong SM-ET coupling (Tables S1 and S2).

Quantification of soil moisture and vegetation effects on ET IAV

In addition to the correlations that indicating the coupling strength, we further quantify the magnitude of SM and LAI control on ET variability. We find that LAI variability induces ET change on a broader coverage than SM, ranging from 60°S to 60°N; meanwhile SM-induced ET IAV change is mostly restricted within 40°S to 40°N (Figures 3A and 3B). Both the LAI and SM effect are weak at the equator and near the two poles. The LAI influence increases as the latitude decreases and reaches the strongest influence along the two sides of the equator. Meanwhile, SM shows a similar trend but a smaller magnitude in the



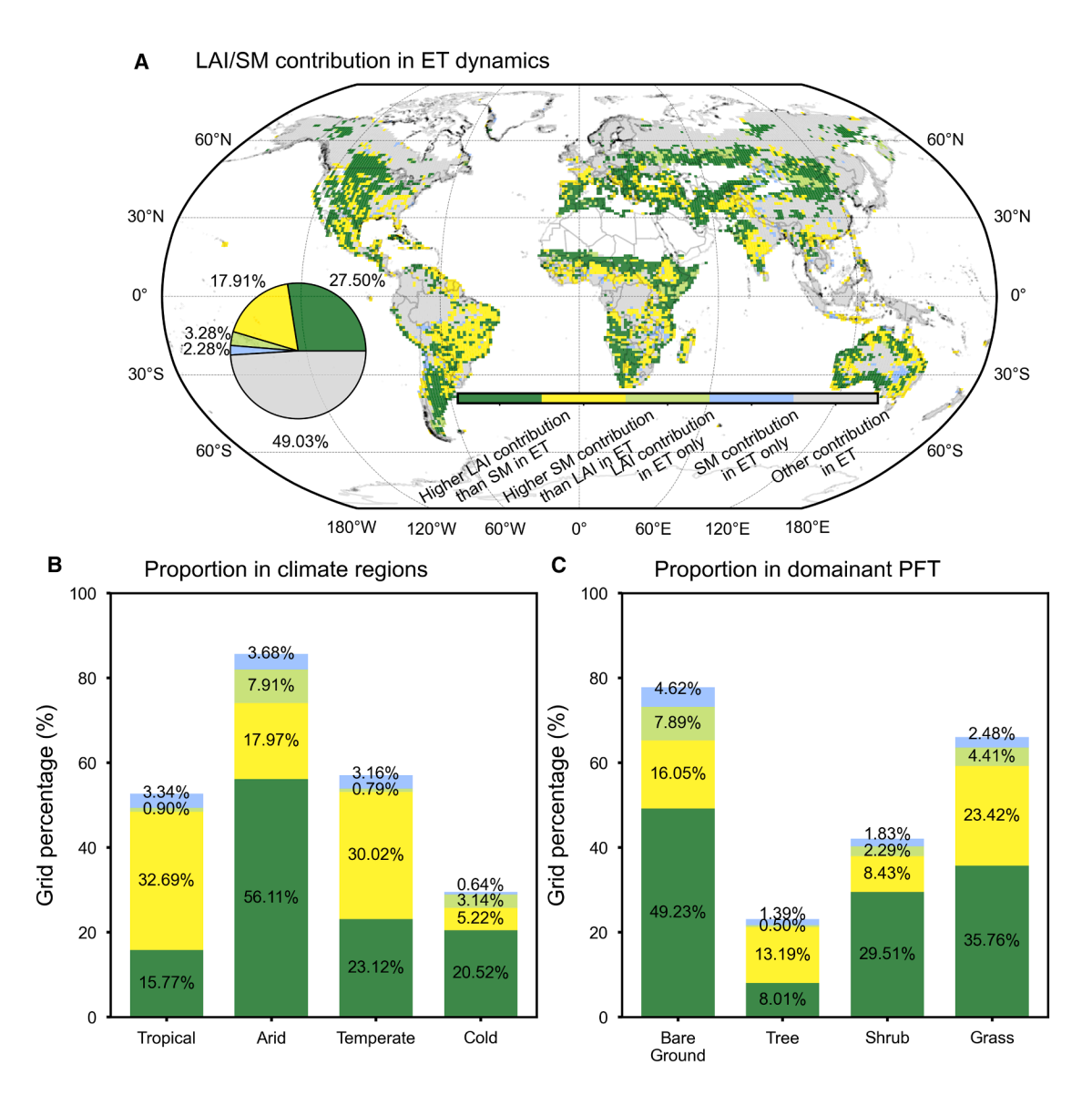


Figure 2. Classification of SM/LAI contribution on ET dynamics

(A) Five classifications based on the relative contribution of LAI and SM on ET dynamics. Grids with r(ET; SM; LAI) < 0.6 are classified as "Other contribution in ET." The inset figure shows the grid percentage of the five categories.

(B and C) The bar plots show the grid percentage of the four categories (except "Other contributes in ET") in different (B) climate regions and (C) dominant plant functional types (PFT).

The colors in the bar plots correspond with the four categories in (A). The numbers indicate percentages of each category.

northern hemisphere and a comparative maximum value in the southern hemisphere along the equator (Figure 3C).

Within different climate regions, the largest difference between the LAI and the SM effect are found in arid regions—where LAI-induced changes in ET IAV average 0.083 \pm 0.062 mm day $^{-1}$, relating to the strong LAI effect in southern South America, central Africa, and Australia. The mean SM-induced ET changes are 0.060 \pm 0.055 mm day $^{-1}$. Because LAI has stronger effects in mid-to-high latitude regions than SM, vegetation-induced changes on ET IAV are 45% and 103% stronger than SM-induced ET IAV changes in temperate and cold regions, respectively (Figure 3D).

The SM-ET coupling and vegetation-ET coupling are most evident in low-precipitation areas (annual mean precipitation (AMP) $< 1,500\,$ mm). Furthermore, SM-ET coupling is more concentrated in areas with high temperatures (annual mean temperature (AMT) $> 20^{\circ}\text{C}$), corresponding with the latitudinal and climatic patterns (Figures S5A and S5B). Strong vegetation-ET coupling regions are characterized by low LAI values, especially over grasslands where LAI-induced ET IAV changes of 0.068 \pm 0.069 mm day $^{-1}$ —compared with 0.040 \pm 0.050 mm day $^{-1}$ for SM-induced ET IAV changes (Figures S5C, S5D, and 3E). Similarly, SM-ET coupling is most obvious in relatively low SM areas, covering locations of both high and low LAI values but exhibiting





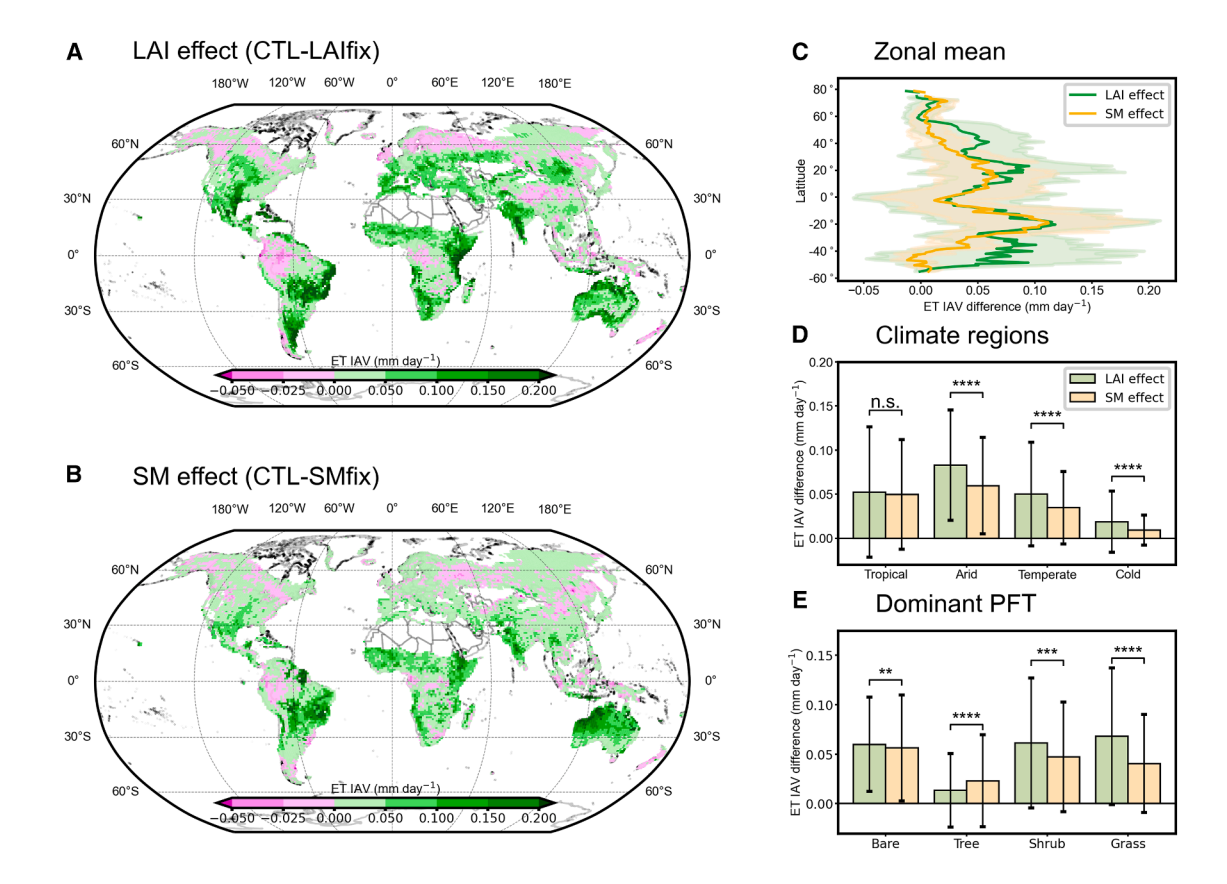


Figure 3. Spatial distribution of effects of SM and LAI on ET IAV

- (A) The difference of ET IAV between CTL and LAIfix.
- (B) The difference in ET IAV between CTL and SMfix.
- (C) The zonal mean of ET IAV difference for CTL and LAlfix, and for CTL and SMfix. Green and orange shading refers to one standard error of the zonal mean for LAI and SM, respectively.

a smaller magnitude than vegetation-ET coupling in low-LAI regions. Therefore, stronger SM-ET coupling occurs in forests than vegetation-ET coupling (0.023 \pm 0.046 mm day $^{-1}$ of SM-induced ET IAV change compared with 0.013 \pm 0.037 mm day $^{-1}$ of LAI-induced ET IAV change); and weaker SM-ET coupling is associated with the bare ground, shrublands, and grasslands (Figures S5C, S5D, and 3E).

Soil moisture-vegetation interactions on ET components

To further investigate how variability in SM and LAI, as well as their interactions, influence ET change, we analyze the individual ET components. Specifically, we examine soil evaporation, canopy interception, and transpiration across three model simulations: the LAI effect (CTL minus LAIfix) and the SM effect (CTL minus SMfix) (Figure 4). Vegetation mainly affects ET IAV by modulating the variability of transpiration, which shows considerable spatial variability (Figures 4A–4C). The transpiration pattern is possibly related to regions dominated by shrublands and grasslands with relatively low LAI values. This pattern likely reflects the high water use efficiency and rapid climate respon-

siveness of these ecosystems, where small changes in LAI can trigger large shifts in transpiration.²⁵ In areas where AMT >20°C and AMP <1500 mm, LAI variability increases the IAV of transpiration (maximum increment: 0.17 mm day⁻¹; mean: 0.092 mm day⁻¹) and reduces the IAV of soil evaporation (maximum reduction: -0.020 mm day⁻¹; mean: -0.0038 mm day⁻¹). These trends indicate higher control of LAI on ET IAV through transpiration, resulting in a smaller proportion of water directly evaporated by soil, which reduces the SM contribution to ET IAV. In areas where 15°C < AMT <30°C and 1500 mm < AMP <2500 mm, LAI variability not only regulates ET through transpiration but also promotes IAV of soil evaporation (maximum value: 0.038 mm day⁻¹). The similar characteristics are also displayed in areas where AMT <10°C and AMP <1000 mm (maximum soil evaporation increase: 0.039 mm day⁻¹). This influence is possibly due to the LAI shading effect²⁶ that induces soil evaporation variability and stemflow-root channelization which facilitates water infiltration, thus affecting SM.²⁷ In areas where AMT >20°C and AMP >2500 mm, the LAI influence on SM becomes weak and insignificant. The transpiration enhancement decreases to 0.011 mm day⁻¹ on average, which



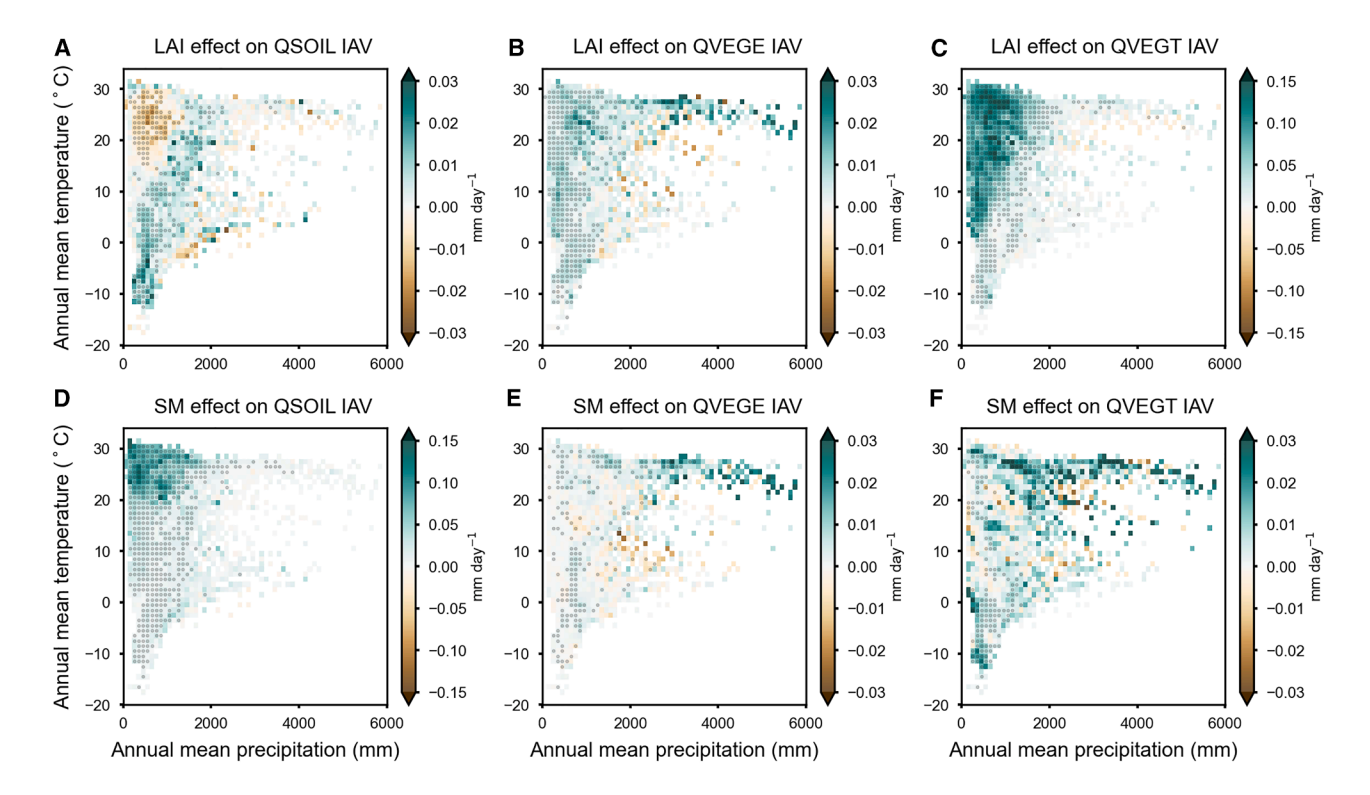


Figure 4. SM and LAI effect on ET components

(A–C) Difference of CTL and LAlfix on the IAV of soil evaporation (QSOIL, A), interception (QVEGE, B), and transpiration (QVEGT, C). (D–F) Also shown is the difference of CTL and SMfix on the IAV of QSOIL (D), QVEGE (E), and QVEGT (F). Values are binned as the function of 30-year mean precipitation and temperature. The black dots denote mean values statistically different from zero using t test at p < 0.05.

is comparable to the canopy interception over the area (mean value: 0.010 mm day⁻¹).

The regulation of SM on ET IAV is directly associated with the modulation of soil evaporation variability, with the highest effect occurring in areas with high temperature (AMT >20°C) and low precipitation (AMP <2000 mm; mean increase in soil evaporation IAV: 0.072 mm day⁻¹; Figure 4D). Compared with LAI-induced change in transpiration, the SM effect on soil evaporation is relatively smaller. Meanwhile, SM also displays vegetation interaction by affecting canopy interception and transpiration at a smaller magnitude (Figures 4E and 4F). In areas where AMT >20°C and AMP >2000 mm, the variation of SM promotes both the variability of plant canopy evaporation (mean value: 0.010 mm day⁻¹) and plant transpiration (mean value: 0.014 mm day⁻¹), supporting the conclusion of the SM effect on canopy conductance in tropical forests.²⁸ The indirect SM effects on ET (by affecting vegetation transpiration and evaporation) are not limited in water-abundant regions, but also in other areas. For example, the enhancement of transpiration IAV is also observed in areas where AMP <2,000 mm. This suggests the widespread control of SM on plant stomatal conductance in regions where precipitation is limited.²⁹

DISCUSSION AND IMPLICATIONS

We find that SM dominates ET variation in most of the previously defined SM coupling hotspots in transitional climate zones of the

low-latitude, such as India, central North America, and central Africa.¹³ This is consistent with the spatial patterns of strong SM-ET coupling strength using various data sources in previous studies. 11,30-32 Meanwhile, in most of the arid and cold regions whose ET variation is strongly coupled with LAI and SM, LAI plays the leading role in regulating ET, which is in agreement with the patterns derived in a past study.33 These findings are not affected by the choice of climate classification method, as we further performed our analysis classified based on aridity index, using the Global-Al_PET_v3 dataset34 (Figure S6). The combined effect of SM and LAI is the strongest in areas with the highest aridity and weakens as aridity decreases (Figure S7A). LAI maintains the dominant role in ET variation in all arid areas (from hyper arid to dry sub-humid) and exerts a higher impact than SM in regulating ET IAV (Figures S7B and S7C).

Separate experiments were conducted to identify the spatial patterns and quantify SM and LAI on ET IAV, respectively. Uncertainty exists on whether the use of standard deviation can represent the ET variation controlled by SM/LAI. To test the robustness of using standard deviation as a measurement of ET IAV, we analyzed ET sensitivity to SM and LAI. The results show that regions with high ET sensitivity to either SM or LAI correspond well with regions exhibiting large ET IAV changes induced by SM or LAI variability (Figure S8). This confirms that standard deviation can effectively capture the magnitude of ET IAV and its correspondence with SM (LAI) dynamics. We also

iScience Article



compare the SM effect on ET with results from previously conducted experiments in the Land Surface, Snow, and Soil Moisture Model Intercomparison Project (LS3MIP).35 In LS3MIP, six participating models performed simulations in which SM dynamics were replaced with their respective climatological values. Comparing SM effect on ET IAV in our simulation (CTL minus SMfix) and the mean value of the six models (historical run minus fixed SM run) shows that our results are in agreement with model ensembles in most of the climate zones and dominant PFTs (Figure S9). Although our simulation presents smaller values compared to the model ensemble data in arid regions and shrublands, the overall trend is successfully captured. For example, our simulation and the model ensemble data both demonstrate the highest value in arid regions and the secondhighest value in tropical regions, reflecting consistency in the trend despite differences in specific magnitudes. The SM effects on precipitation IAV in our study also align with the model ensembles, suggesting that the ET changes are due to surface processes instead of the indirect effects of climate feedback (Figure S10).

Our study highlights the importance of considering both SM and LAI effects in the terrestrial segments for the LAC. In land-atmosphere interactions, a large portion of the current change of climate IAV may be attributed to LAC associated with SM-ETclimate and vegetation-ET-climate interactions. As global warming continues, transitional regimes are expected to emerge in high latitudes, suggesting stronger SM-atmosphere coupling over the area.³⁶ Combined with the vegetation-ET coupling and vegetation effect on promoting soil evaporation variability over high latitudes, climate interannual variability may be further amplified through LAC in these areas, increasing the risks of extreme weather events. As global vegetation greening is predicted to continue during the 21st century,37 the uncertainty of the complex SM-vegetation interaction in LAC may expand in the future, considering the current increasing vegetation sensitivity to drying SM.38 Moreover, as arid region water cycles are strongly coupled with carbon cycle, 39,40 our findings provide insights into variability in regional carbon cycles. Accurate SM and LAI simulation and improved representation of SM-vegetation interactions will advance climate projections under future climate change scenarios.

Conclusions

Our study suggests that LAC may have a bigger impact on climate than previously thought. As these couplings intensify, they could lead to more frequent or severe climate extremes in the future. Our findings show that both SM and vegetation play important roles in shaping evapotranspiration (ET) variability across the globe. While SM remains the dominant factor on ET dynamics in the low-latitude regions, vegetation has a surprisingly strong influence in arid regions and high-latitude wet regions—especially through its control over transpiration. We also find that the way vegetation and SM interact is not uniform: in high-temperature and low-precipitation areas, vegetation tends to reduce soil evaporation, but in other climates, it can increase it. Meanwhile, SM influences not just evaporation from the soil but also canopy processes like interception and transpiration, especially in warmer and wetter areas. By high-

lighting the complex and regionally diverse ways in which land conditions influence climate, this study points to the need for models and climate assessments to better account for the joint effects of vegetation and SM.

Limitations of the study

There are also uncertainties and limitations in our study. We focus on the coupling between land conditions of SM and LAI on ET variability, however, other factors involved in the coupling with ET and atmospheric variables such as vapor pressure deficit, temperature, and precipitation⁴¹ were not included in this study. How SM and LAI interact with these factors directly or indirectly remain to be explored. Meanwhile, our study is also limited by the deficiencies in the earth system model. Vegetation and SM feedbacks on climate are highly dependent on ET sensitivity to LAI and SM changes, within which the fraction of transpiration in ET (T/ET) plays an important role. The lack of accurate representation of transpiration partitioning in current earth system models may cause bias to the estimation of SM and vegetation feedbacks on ET.^{42,43}

RESOURCE AVAILABILITY

Lead contact

Requests for further information and resources should be directed to the lead contact, Zhenzhong Zeng (zengzz@sustech.edu.cn).

Material availability

This study did not generate new materials.

Data and code availability

The GLEAM dataset can be retrieved from https://www.gleam.eu/. The global PEW land evapotranspiration dataset is available at https://data.tpdc.ac.cn/en/data/bc567cf8-4fe6-4d2f-8e36-2262bdb3c2ff. The TRENDY dataset is available on request from https://blogs.exeter.ac.uk/trendy/. The CMIP6 historical and LS3MIP data are retrieved from https://pcmdi.llnl.gov/CMIP6/. The Global-Al_PET_v3 dataset can be retrieved from https://figshare.com/articles/dataset/Global_Aridity_Index_and_Potential_Evapotranspiration_ET0_Climate_Database_v2/7504448/5. All generated data from CESM2 are available from the corresponding author on request.

Codes and documentations for the CESM model are publicly available at https://www.cesm.ucar.edu:/models/cesm2. Model outputs were processed using Python 3.7. The python scripts can be retrieved from the corresponding author upon request.

ACKNOWLEDGMENTS

This study was supported by the start-up fund provided by Shenzhen Science and Technology project for ustainable Development in Special Innovation (KCXFZ20230731093403008), Guangdong Basic and Applied Basic Research Foundation (no. 2022A1515240070), the National Natural Science Foundation of China (no. 42071022), the Shenzhen Key Laboratory of Precision Measurement and Early Warning Technology for Urban Environmental Health Risks (ZDSYS20220606100604008), the funding agencied of Zhejiang Province and Ningbo Municipality through the program "Novel Technologies for Joint Pollution Reduction and Carbon Sequestration", and the start-up and high-level special funds provided by the Southern University of Science and Technology (29/Y01296602; 29/Y01296122; 29/Y01296222; G030290001). We thank the Center for Computational Science and Engineering at the Southern University of Science and Technology for providing computing resources.





AUTHOR CONTRIBUTIONS

Z.Z. and S.L. designed the research; S.L. and X.H. conducted simulations; X.H. interpreted the results and wrote the manuscript with contributions from all co-authors; X.H., S.L., A.D.Z., and Z.Z. edited the manuscript.

DECLARATION OF INTERESTS

The authors declare no competing interests.

STAR*METHODS

Detailed methods are provided in the online version of this paper and include the following:

- KEY RESOURCES TABLE
- METHOD DETAILS
 - Fully-coupled Earth System Model simulation
 - o Model performance
 - o Computation of ET IAV
 - SM-vegetation-ET coupling and relative contribution
- QUANTIFICATION AND STATISTICAL ANALYSIS

SUPPLEMENTAL INFORMATION

Supplemental information can be found online at https://doi.org/10.1016/j.isci. 2025.113008.

Received: January 13, 2025 Revised: May 21, 2025 Accepted: June 23, 2025 Published: June 25, 2025

REFERENCES

- Seneviratne, S.I., Corti, T., Davin, E.L., Hirschi, M., Jaeger, E.B., Lehner, I., Orlowsky, B., and Teuling, A.J. (2010). Investigating soil moisture-climate interactions in a changing climate: a review. Earth Sci. Rev. 99, 125–161.
- Seneviratne, S.I., Lüthi, D., Litschi, M., and Schär, C. (2006). Land-atmosphere coupling and climate change in Europe. Nature 443, 205–209.
- Yang, Y., Roderick, M.L., Guo, H., Miralles, D.G., Zhang, L., Fatichi, S., Luo, X., Zhang, Y., McVicar, T.R., Tu, Z., et al. (2023). Evapotranspiration on a greening Earth. Nat. Rev. Earth Environ. 4, 626–641.
- Lee, T.H., Lo, M.H., Chiang, C.L., and Kuo, Y.N. (2023). The maritime continent's rainforests modulate the local interannual evapotranspiration variability. Commun. Earth. Environ. Times 4, 482.
- Berg, A., and Sheffield, J. (2019). Historic and projected changes in coupling between soil moisture and evapotranspiration (ET) in CMIP5 models confounded by the role of different ET components. JGR. Atmospheres 124, 5791–5806.
- Qiao, L., Zuo, Z., Zhang, R., Piao, S., Xiao, D., and Zhang, K. (2023). Soil moisture–atmosphere coupling accelerates global warming. Nat. Commun. 14, 4908.
- Seo, Y.W., and Ha, K.J. (2022). Changes in land-atmosphere coupling increase compound drought and heatwaves over northern East Asia. NPJ Clim. Atmos. Sci. 5, 100.
- Zhang, J., Wu, L., and Dong, W. (2011). Land-atmosphere coupling and summer climate variability over East Asia. J. Geophys. Res. 116, D05117.
- Dirmeyer, P.A., Balsamo, G., Blyth, E.M., Morrison, R., and Cooper, H.M. (2021). Land-atmosphere interactions exacerbated the drought and heatwave over northern Europe during summer 2018. AGU Adv. 2, e2020AV000283.
- Chen, Y., and Wang, A. (2024). Role of land-atmosphere coupling in persistent extreme climate events in eastern China in summer 2022. Atmosph. Ocean. Sci. Lett. 17, 100419.

- Dirmeyer, P.A. (2011). The terrestrial segment of soil moisture-climate coupling. Geophys. Res. Lett. 38, L16702.
- Han, D., Wang, G., Liu, T., Xue, B.L., Kuczera, G., and Xu, X. (2018). Hydroclimatic response of evapotranspiration partitioning to prolonged droughts in semiarid grassland. J. Hydrol. X. 563, 766–777.
- Koster, R.D., Sud, Y.C., Guo, Z., Dirmeyer, P.A., Bonan, G., Oleson, K.W., Chan, E., Verseghy, D., Cox, P., Davies, H., et al. (2006). GLACE: the global land-atmosphere coupling experiment. Part I: overview. J. Hydrometeorol. 7, 590–610.
- Guo, Z., Dirmeyer, P.A., Koster, R.D., Sud, Y.C., Bonan, G., Oleson, K.W., Chan, E., Verseghy, D., Cox, P., Gordon, C.T., et al. (2006). GLACE: the global land-atmosphere coupling experiment. Part II: analysis. J. Hydrometeorol. 7, 611–625.
- Lian, X., Jeong, S., Park, C.E., Xu, H., Li, L.Z.X., Wang, T., Gentine, P., Peñuelas, J., and Piao, S. (2022). Biophysical impacts of northern vegetation changes on seasonal warming patterns. Nat. Commun. 13, 3925.
- Yu, L., Xue, Y., and Diallo, I. (2021). Vegetation greening in China and its effect on summer regional climate. Sci. Bull. 66, 13–17.
- Williams, I.N., and Torn, M.S. (2015). Vegetation controls on surface heat flux partitioning, and land-atmosphere coupling. Geophys. Res. Lett. 42, 9416–9424.
- Tang, Q., Xie, S., Zhang, Y., Phillips, T.J., Santanello, J.A., Cook, D.R., Riihimaki, L.D., and Gaustad, K.L. (2018). Heterogeneity in warm-season land-atmosphere coupling over the US Southern great plains. J. Geophys. Res. Atmos. 123, 7867–7882.
- Forzieri, G., Miralles, D.G., Ciais, P., Alkama, R., Ryu, Y., Duveiller, G., Zhang, K., Robertson, E., Kautz, M., Martens, B., et al. (2020). Increased control of vegetation on global terrestrial energy fluxes. Nat. Clim. Chang. 10, 356–362.
- Lian, X., Piao, S., Li, L.Z.X., Li, Y., Huntingford, C., Ciais, P., Cescatti, A., Janssens, I.A., Peñuelas, J., Buermann, W., et al. (2020). Summer soil drying exacerbated by earlier spring greening of northern vegetation. Sci. Adv. 6. eaax0255
- Feng, X., Fu, B., Zhang, Y., Pan, N., Zeng, Z., Tian, H., Lyu, Y., Chen, Y., Ciais, P., Wang, Y., et al. (2021). Recent leveling off of vegetation greenness and primary production reveals the increasing soil water limitations on the greening Earth. Sci. Bull. 66, 1462–1471.
- 22. Wang, C., Fu, B., Zhang, L., and Xu, Z. (2019). Soil moisture–plant interactions: an ecohydrological review. J. Soils Sediments 19, 1–9.
- 23. Danabasoglu, G., Lamarque, J.F., Bacmeister, J., Bailey, D.A., DuVivier, A.K., Edwards, J., Emmons, L.K., Fasullo, J., Garcia, R., Gettelman, A., et al. (2020). The community earth system model version 2 (CESM2). J. Adv. Model. Earth Syst. 12, e2019MS001916.
- Salmerón, R., García, C.B., and García, J. (2018). Variance inflation factor and condition number in multiple linear regression. J. Stat. Comput. Simul. 88, 2365–2384
- Wei, Z., Yoshimura, K., Wang, L., Miralles, D.G., Jasechko, S., and Lee, X. (2017). Revisiting the contribution of transpiration to global terrestrial evapotranspiration. Geophys. Res. Lett. 44, 2792–2801.
- 26. Ge, Z.M., Zhou, X., Kellomäki, S., Peltola, H., and Wang, K.Y. (2011). Climate, canopy conductance and leaf area development controls on evapotranspiration in a boreal coniferous forest over a 10-year period: a united model assessment. Ecol. Modell. 222, 1626–1638.
- Ludwig, J.A., Wilcox, B.P., Breshears, D.D., Tongway, D.J., and Imeson, A.C. (2005). Vegetation patches and runoff–erosion as interacting ecohydrological processes in semiarid landscapes. Ecology 86, 288–297.
- Harris, P.P., Huntingford, C., Cox, P.M., Gash, J.H.C., and Malhi, Y. (2004).
 Effect of soil moisture on canopy conductance of Amazonian rainforest.
 Agric. For. Meteorol. 122, 215–227.
- Tobin, R.L., and Kulmatiski, A. (2018). Plant identity and shallow soil moisture are primary drivers of stomatal conductance in the savannas of Kruger National Park. PLoS One 13, e0191396.

iScience Article



- Berg, A., and Sheffield, J. (2018). Soil moisture–evapotranspiration coupling in CMIP5 models: relationship with simulated climate and projections. J. Clim. 31, 4865–4878.
- Zhou, J., Yang, K., Dong, J., Crow, W.T., Lu, H., Zhao, L., Feng, H., Tian, J., Ma, X., Tian, X., and Jiang, Y. (2025). Mapping global soil moisture and evapotranspiration coupling strength based on a two-system method and multiple data sources. Water Resour. Res. 61, e2023WR036847.
- Lei, F., Crow, W.T., Holmes, T.R.H., Hain, C., and Anderson, M.C. (2018).
 Global investigation of soil moisture and latent heat flux coupling strength.
 Water Resour. Res. 54, 8196–8215.
- Chen, H., and Zeng, X.D. (2012). The impacts of the interannual variability
 of vegetation on the interannual variability of global evapotranspiration: a
 modeling study. Atmos. Oceanic Sci. Lett. 5, 225–230.
- 34. Zomer, R.J., Xu, J., and Trabucco, A. (2022). Version 3 of the global aridity index and potential evapotranspiration database. Sci. Data 9, 409.
- van den Hurk, B., Kim, H., Krinner, G., Seneviratne, S.I., Derksen, C., Oki, T., Douville, H., Colin, J., Ducharne, A., Cheruy, F., et al. (2016). LS3MIP (v1.0) contribution to CMIP6: the land surface, snow and soil moisture model intercomparison project - aims, setup and expected outcome. Model Dev. 9, 2809–2832.
- **36.** Hsu, H., and Dirmeyer, P.A. (2023). Soil moisture-evaporation coupling shifts into new gears under increasing CO₂. Nat. Commun. *14*, 1162.
- Piao, S., Wang, X., Park, T., Chen, C., Lian, X., He, Y., Bjerke, J.W., Chen, A., Ciais, P., Tømmervik, H., et al. (2019). Characteristics, drivers and feed-backs of global greening. Nat. Rev. Earth Environ. 1, 14–27.
- Li, W., Migliavacca, M., Forkel, M., Denissen, J.M.C., Reichstein, M., Yang, H., Duveiller, G., Weber, U., and Orth, R. (2022). Widespread increasing vegetation sensitivity to soil moisture. Nat. Commun. 13, 3959.
- Kannenberg, S.A., Anderegg, W.R.L., Barnes, M.L., Dannenberg, M.P., and Knapp, A.K. (2024). Dominant role of soil moisture in mediating carbon and water fluxes in dryland ecosystems. Nat. Geosci. 17, 38–43.
- Zhang, L., Xiao, J., Zheng, Y., Li, S., and Zhou, Y. (2020). Increased carbon uptake and water use efficiency in global semi-arid ecosystems. Environ. Res. Lett. 15, 034022.
- Xue, Y., Xue, Y., Chen, M., and Zhang, Y. (2025). Exploring the contribution of vegetation and climate factors to changes in terrestrial evapotranspiration in China. Sci. Total Environ. 967, 178808.

- 42. Wang, D., and Zeng, Z. (2024). Urgent need to improve modelled sensitivity of evaporation to vegetation change. Nat. Water 2, 211–214.
- Feng, H., Wu, Z., Dong, J., Zhou, J., Brocca, L., and He, H. (2023). Transpiration Soil evaporation partitioning determines inter-model differences in soil moisture and evapotranspiration coupling. Remote Sens. Environ. 298, 113841.
- Kennedy, D., Swenson, S., Oleson, K.W., Lawrence, D.M., Fisher, R., Lola da Costa, A.C., and Gentine, P. (2019). Implementing plant hydraulics in the community land model, version 5. J. Adv. Model. Earth Syst. 11, 485–513.
- Miralles, D.G., Holmes, T.R.H., De Jeu, R.A.M., Gash, J.H., Meesters, A.G.
 C.A., and Dolman, A.J. (2011). Global land-surface evaporation estimated from satellite-based observations. Hydrol. Earth Syst. Sci. 15, 453–469.
- Martens, B., Miralles, D.G., Lievens, H., Van Der Schalie, R., De Jeu, R.A.M., Fernández-Prieto, D., Beck, H.E., Dorigo, W.A., and Verhoest, N.E.C. (2017). GLEAM v3: satellite-based land evaporation and root-zone soil moisture. Geosci. Model Dev. 10, 1903–1925.
- Fu, J., Wang, W., Shao, Q., Xing, W., Cao, M., Wei, J., Chen, Z., and Nie, W. (2022). Improved global evapotranspiration estimates using proportionality hypothesis-based water balance constraints. Remote Sens. Environ. 279. 113140.
- Eyring, V., Bony, S., Meehl, G.A., Senior, C.A., Stevens, B., Stouffer, R.J., and Taylor, K.E. (2016). Overview of the coupled model intercomparison project phase 6 (CMIP6) experimental design and organization. Geosci. Model Dev. 9, 1937–1958.
- Sitch, S., Friedlingstein, P., Gruber, N., Jones, S.D., Murray-Tortarolo, G., Ahlström, A., Doney, S.C., Graven, H., Heinze, C., Huntingford, C., et al. (2015). Recent trends and drivers of regional sources and sinks of carbon dioxide. Biogeosciences 12, 653–679.
- Peel, M.C., Finlayson, B.L., and McMahon, T.A. (2007). Updated world map of the Köppen-Geiger climate classification. Hydrol. Earth Syst. Sci. 11, 1633–1644.
- Ebrahimi-Khusfi, Z., Mirakbari, M., and Khosroshahi, M. (2020). Vegetation response to changes in temperature, rainfall, and dust in arid environments. Environ. Monit. Assess. 192, 691.
- Dai, X., Yu, Z., Matheny, A.M., Zhou, W., and Xia, J. (2022). Increasing evapotranspiration decouples the positive correlation between vegetation cover and warming in the Tibetan plateau. Front. Plant Sci. 13, 974745.





STAR*METHODS

KEY RESOURCES TABLE

REAGENT or RESOURCE	SOURCE	IDENTIFIER
Deposited data		
Global Land Evaporation Amsterdam Model version 3.8a	European Space Agency, Ghent University, and Vrije Universiteit Amsterdam	https://www.gleam.eu/
Global PEW Land Evapotranspiration Dataset	National Tibetan Plateau Data Center	https://data.tpdc.ac.cn/en/data/bc567cf8-4fe6-4d2f-8e36-2262bdb3c2ff
"Trends in the land carbon cycle" project (TRENDY-v11)	Global Carbon Project	https://blogs.exeter.ac.uk/trendy/
CMIP6 historical dataset	World Climate Research Program (WCRP)	https://pcmdi.llnl.gov/CMIP6/
LS3MIP dataset	World Climate Research Program (WCRP)	https://pcmdi.llnl.gov/CMIP6/
Global Aridity Index and Potential Evapo-Transpiration (ET0) Database v3 (Global-Al_PET_v3)	Consortium for Spatial Information (CGIAR-CSI)	https://figshare.com/articles/dataset/Global_ Aridity_Index_and_Potential_Evapotranspiration_ ET0_Climate_Database_v2/7504448/5
Software and algorithms		
CESM v2.1.3	National Center for Atmospheric Research (NCAR)	https://www.cesm.ucar.edu:/models/cesm2
Python 3.7	Open-source software	https://www.python.org/

METHOD DETAILS

Fully-coupled Earth System Model simulation

We characterize and decouple the SM-vegetation interaction on ET using the fully-coupled CESM model (version 2.1.3), which consists of the atmosphere component Community Atmosphere Model Version 6 (CAM6), the ocean component Parallel Ocean Program Version 2 (POP2), the sea ice component Los Alamos Sea Ice Model Version 5.1.2 (CICE5), the land ice component Community Ice Sheet Model Version 2.1 (CISM2.1), the land component Community Land Model Version 5 (CLM5), and the river component Model for Scale Adaptive River Transport (MOSART). The coupler Common Infrastructure for Modeling the Earth (CIME) controls the state and flux changes between these components.²³ The CESM2 is improved in historical simulations compared with the previous model version and observation data.²³ The model has contributed to the Coupled Model Intercomparison Project Phase 6 (CMIP6). Specifically, for the land component, the CLM5 is implemented with an updated soil-plant-atmosphere continuum model and reduces transpiration and SM bias, which improves simulations on land-climate feedbacks.⁴⁴

The description of the experimental design is shown in Figure S1. Four simulations were conducted in total, with one simulation (BGC-run) providing the input data for the rest of the three experiments (CTL, LAIfix, and SMfix). The outputs from these three experiments were applied to study the role of vegetation and SM in ET variability. Since the historical simulations end in 2014, the study period was restricted to the last 30 years of the historical runs, i.e., from 1985 to 2014. All four experiments were configured with the fully coupled historical ("BHIST") component set without dynamic crop management, and forced by prognostic atmospheric CO_2 , which was computed from surface fluxes of the land and the ocean model. All components (land, ocean, atmosphere, etc.) were active in "BHIST" simulations to enable full interactions between the components to provide more realistic climate simulations. The grid resolution was set as "f09_g17_gl4" with a model resolution of $0.9^{\circ} \times 1.25^{\circ}$ for land and the atmosphere. The historical simulation of active biogeochemistry (BGC) mode starting from 1850 was first run (BGC-run) to produce the monthly dynamic data of LAI (BGC-LAI) and SM (BGC-SM) from 1980 to 2014. The monthly climatological LAI and SM time series were calculated from their dynamic series. The dynamic and climatological series were used as input data for the three experiments.

To modify LAI and SM series in CESM, all three experiments were conducted using the satellite phenology (SP) mode with prescribed LAI and SM monthly series and run between 1980 and 2014. The differences between the three experiments were the prescribed SM and LAI conditions. The control (CTL) run was prescribed with the dynamic monthly BGC-LAI and BGC-SM data. In the LAI fix run, the variability of LAI was fixed by prescribing the monthly climatological time series of BGC-LAI, and the SM variability was maintained with prescribed monthly dynamic BGC-SM. For the SMfix run, the LAI variability was retained by prescribing LAI with monthly dynamic BGC-LAI, and SM variability was fixed by prescribing the monthly climatology of BGC-SM. All three experiments began from 1980 as branch runs of the BGC-run with identical initial states. The difference between CTL and LAI (SMfix) then reveals the roles of LAI (SM) variability on climate. The first 5 years were excluded in the analysis.

iScience Article



Model performance

We first used near-observation ET data to evaluate CESM performance on ET simulation. The 30-year annual mean ET and ET IAV of the CTL simulation were compared with the Global Land Evaporation Amsterdam Model version 3.8a (GLEAM)^{45,46} and the Global PEW Land Evapotranspiration Dataset (PEW) developed by the National Tibetan Plateau Data Center.⁴⁷ Based on satellite and reanalysis data, GLEAM estimates global ET and individual components at a spatial resolution of 0.25° spanning from 1980 to 2022. The PEW dataset is derived from the Global Land Surface Satellite (GLASS) data and reanalysis products using a modified Priestly-Taylor equation, with a spatial resolution of 0.1° and a time period of 1982–2018. The annual mean ET in GLEAM dataset and the monthly mean ET in PEW dataset were derived. The annual series of the two near-observation datasets between 1985 and 2014 were resampled to the spatial resolution of the CTL and compared with the CTL grids.

The Spatial patterns of the 30-year average and IAV of ET in CTL simulation showed consistency with GLEAM and PEW (Figure S11). The CTL produced consistent ET means in areas such as tropical forests, East Asia, and North America, with high spatial correlation with both GLEAM (r = 0.90) and PEW (r = 0.93, Figures S11A, S11C, and S11E). The ET IAV generally exhibited smaller consistency than the ET average, but the spatial distribution of ET IAV was well-captured including North America, Australia, and South America, with a spatial correlation of approximately 0.6 (r = 0.58 between GLEAM and CTL, r = 0.61 between PEW and CTL; Figures S11B, S11D, and S11F). We also evaluated the overall global performance of ET simulations with the two observation-based datasets and model ensembles, including 54 models in the CMIP6⁴⁸ and 15 dynamic global vegetation models (DGVMs) in the "Trends in the land carbon cycle" project version 11 (TRENDY⁴⁹; Figure S12). The CTL simulated ET mean (1.86 mm day⁻¹) was within the range of near-observation datasets and model ensembles (1.61–1.95 mm day⁻¹). The global IAV of CTL was close to the CMIP6 ensemble mean, with a difference of less than 0.01 mm day⁻¹, confirming the ability of CESM2 in the ET simulation.

Computation of ET IAV

We defined the IAV of ET as the standard deviation of annual mean values over the 30 years, following Seneviratne et al.² To avoid trend-induced inflation on the standard deviation, the time series of the climate variables were linearly de-trended. The regional calculations among climate regions and dominant PFT were based on the Koppen-Geiger climate classification⁵⁰ and the land cover in the CESM2, respectively (Figure S2). The grids were area-weighted regionally and globally.

SM-vegetation-ET coupling and relative contribution

Traditional metrics usually measure the impacts of one factor on another one factor (e.g., correlations between SM and temperature, correlations between LAI and evaporative factor, and correlations between SM and ET). Here we adopted the multiple correlation coefficient to consider the combined effects of multiple factors on one factor and conducted multiple linear regression to separate their individual impacts. The coupling strength of SM and vegetation on ET in the CTL simulation was estimated by the multiple correlation coefficient (r)¹⁸:

$$r_{(\text{ET;SM,LAI})} = \frac{\sqrt{r^2(ET,SM) + r^2(ET,LAI)} - 2 \times r(ET,SM) \times r(ET,LAI) \times r(SM,LAI)}}{\sqrt{1 - r^2(SM,LAI)}} \tag{Equation 1}$$

where r(ET,SM), r(ET,LAI), and r(SM,LAI) denote the Pearson's correlation coefficient between the variables in parentheses. Larger $r_{(ET;SM,LAI)}$ values indicate higher strength of SM-LAI combined effects on ET IAV. The contributions of SM and LAI were determined based on multiple linear regression. The autocorrelation and multicollinearity of annual SM and LAI were first examined using the Variance Inflation Factor (VIF) analysis²⁴ to ensure the independence of the variables. VIF values between 5 and 10 suggest moderate collinearity and values over 10 suggest severe collinearity, which will require elimination in the analysis. For each grid, the VIF value was calculated as:

$$VIF_j = \frac{1}{1 - R_j^2}$$
 (Equation 2)

where VIF_j refers to the VIF values of SM or LAI; and R_j^2 denotes the R-square value of the regression of SM (LAI) on LAI (SM). ⁵¹ The VIF values of SM and LAI showed little difference, with nearly all VIF values below 5, suggesting weak correlation and no statistically significant multicollinearity between annual SM and LAI series, which enabled the application of multiple linear regression (Figure S3). The multiple linear regression was constructed as:

$$ET = b_1 \times SM + b_2 \times LAI + b_0$$
 (Equation 3)

where b_i represent partial regression coefficients of SM, LAI, and other factors, respectively. To compare the importance of SM and LAI, the partial regression coefficients were standardized:

$$B_i = b_i \times \frac{\sigma_x}{\sigma_y}$$
 (Equation 4)

where B_i denotes the standardized regression coefficient and σ_x denotes the standard deviation of SM or LAI, and σ_y represents the standard deviation of ET. 18





The dominance of SM and LAI on ET was determined based on the B_i , as shown in Figure 2. Positive B_i values indicate SM or LAI contribution to ET, as the increase (decrease) of SM or LAI increases (reduces) ET; and negative values denote ET control on SM or LAI, as increased (decreased) ET reduces (retains or increases) SM content or limits (promotes) vegetation growth. ^{1,52} If both B_{SM} and B_{LAI} are positive and B_{SM} is larger (smaller) than B_{LAI} , then ET is contributed by both SM and LAI, with SM (LAI) exerting higher contribution. If B_{SM} (B_{LAI}) is positive and B_{LAI} (B_{SM}) is negative, then ET is contributed by SM (LAI) only. If both B_{SM} and B_{LAI} are negative, then ET is affected by other factors.

QUANTIFICATION AND STATISTICAL ANALYSIS

All statistical analyses and data visualization were performed using Python. The analyses included calculations of standard deviation to measure variability, Pearson's correlation coefficient to assess coupling strength, and multiple linear regression to model variable dependencies. Detailed statistical parameters (including statistical test types and *p*-values) are provided in Figures 1, 2, 3, and 4, the figure legends, and the results section.